ACS APPLIED MATERIALS & INTERFACES

www.acsami.org Research Article

Red Fluorescent Carbon Dot Powder for Accurate Latent Fingerprint Identification using an Artificial Intelligence Program

Xiang-Yang Dong, Xiao-Qing Niu, Zheng-Yong Zhang, Ji-Shi Wei, and Huan-Ming Xiong*

Cite This: *ACS Appl. Mater. Interfaces* 2020, 12, 29549−29555 **Read Online**

ACCESS | Metrics & More | Article Recommendations | Supporting Information

ABSTRACT: Development and comparison of the latent fingerprints (LFPs) are two major studies in detection and identification of LFPs, respectively. However, integrated research studies on both fluorescent materials for LFP development and digital-processing programs for LFP comparison are scarcely seen in the literature. In this work, highly efficient red-emissive carbon dots (R-CDs) are synthesized in one pot and mixed with starch to form R-CDs/starch phosphors. Such phosphors are comparable with various substrates and suitable for the typical powder dusting method to develop LFPs. The fluorescence images of the developed LFPs are handled with an artificial intelligence program. For the optimal sample, this program presents an excellent matching score of 93%, indicating that the developed sample has very high similarity with the standard control. Our results are significantly better than the benchmark obtained by the traditional method, and thus, both the R-CDs/starch phosphors and the digital processing program fit well for the practical applications.

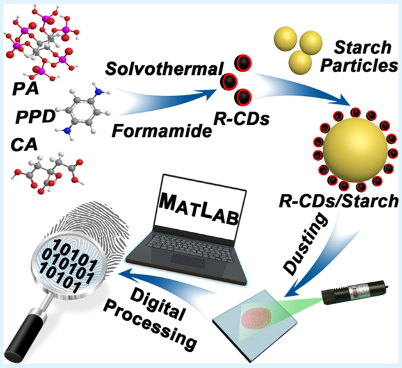

KEYWORDS: *carbon dots, red fluorescence, fingerprint, analysis, artificial intelligence*

1. INTRODUCTION

Since the 19th century, fingerprint analysis has been established as a reliable approach for personal identification. When a finger touches a solid substance, its secretion will be left on the surface with characteristic ridge patterns. In most cases, such patterns are typically called latent fingerprints (LFPs) because their poor optical contrast with the substrates is invisible to naked eyes.[1,2] To detect and identify LFPs, two major studies should be conducted with great care and patience. One is LFP development, which typically involves dusting some dyes to enhance the visual contrast between fingerprints and backgrounds and then recording the patterns by imaging techniques. The other is LFP comparison, which means collecting highly similar patterns from different sources, comparing these patterns using a standard program, and making a reliable identification according to the matching score.[3−6]

So far, plenty of methods have been developed to detect LFPs.[7−10] Among them, fluorescence imaging is a popular approach in which dyes or photoluminescent (PL) nanomaterials are dusted on LFPs to show high-contrast fluorescent signals under light irradiation.[11] For example, magnetic particles,[12] quantum dots,[13] and upconversion nanoparticles (UCNPs)[14] have been employed for LFP development. However, many dye powders, including rhodamines, are apt to adhere on the overall surface of substrates so that fingerprint lines cannot be distinguished clearly. In practical applications, these dyes are always dispersed in a large amount of medium (carrier powder) to realize good fluidity and avoid dye powder stagnation and sticking on the substrates. We also reported a spraying method by carbon dots (CDs) in aqueous solution, which manifests LFPs on impermeable substrates based on the coffee ring effect and the unquenched CD fluorescence in the drying process.[15] However, these methods are often limited by the complex or expensive preparation routes, potential toxicity, destructive detection processes, and poor stability in practical environments.[16] More importantly, in most previous reports, there are only manual LFP comparisons, which are low efficient and rather subjective.[17] For many years, there exist two fields of LFP research studies which have been isolated. One is LFP detection which mainly attracts material scientists to invent various chromogenic reagents or fluorescent dyes, but the subsequent LFP identification procedures in their work are primary, only comparing the images manually. The other is LFP identification which is mainly studied by computer programmers, who design programs to digitalize the images for comparison with the databases but do not know how to obtain a good LFP image from the scenes. To our knowledge, there are no successful reports integrating LFP detection and LFP identification yet. In addition, most of the reports even have no control for LFP comparison. Therefore, developing a new

Received: February 1, 2020
Accepted: June 4, 2020
Published: June 16, 2020

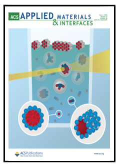

https://dx.doi.org/10.1021/acsami.0c01972
ACS Appl. Mater. Interfaces 2020, 12, 29549−29555

Scheme 1. Preparation Process of R-CDs/Starch Powder and Its Application in LFP Detection

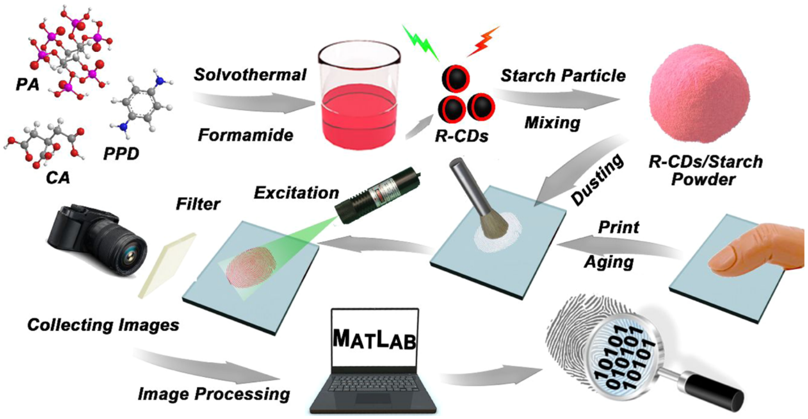

material with high quality to light up LFPs on various substrates by a simple, portable, and safe way, and meanwhile establishing a quantitatively analytical program for comparing LFPs accurately and intuitively, becomes an urgent challenge for the LFP detection and identification.

During the past decade, CDs have been intensively investigated because of their outstanding merits such as facile synthesis, low cost, high yield, stable structure, versatile functions, and good biosafety.[18−21] Although CDs have been widely applied in fluorescence imaging, their applications in LFP detection are rarely reported because of some shortcomings. First, the emission colors of CDs are usually blue or green, which are interfered by the background fluorescence of many substrates, especially under UV light. Second, the conventional CDs show bright fluorescence in solution but solution-casting is not suitable for permeable substrates, such as paper, cloth, and wood.[3,7] Third, when the CD solutions are dried, the fluorescence of CDs is always quenched by aggregation effects.[22] Thus, the typical CD powders do not work in the dusting method which is the most widely used for LFP detection. Although some CD-based hybrid powders were prepared with weak fluorescence recently,[23,24] their LFP identification abilities were poor, and no red fluorescent CD powder has been applied for LFP detection yet. Furthermore, the subsequent LFP identification and comparison with the control have never been studied systematically.

In this work, we developed a simple method to synthesize red-emissive CDs (R-CDs), prepared CD-based phosphors in the large scale by integrating the R-CDs with starch particles, and applied the as-prepared phosphors to detect LFPs on various substrates by the powder-dusting method. Under green light irradiation, the bright red fluorescence of R-CDs lit up LFPs which showed very clear ridge patterns without interference of the background fluorescence. We set up a digital-processing program to identify LFPs objectively, which extracted the detail features of LFPs on different substrates, compared the features with the control accurately, and presented the matching scores using a computer. The highest matching score reached 93%, exceeding the benchmark obtained by the standard police method for LFP identification.

2. EXPERIMENTAL SECTION

2.1. Materials. Citric acid (CA), *p*-phenylenediamine (PPD), phytic acid (PA), formamide acetone, starch, rhodamine 6G, and methanol were obtained from Sinopharm Chemical Reagent Co. (China). All chemicals were used as received. Ultrapure water (Milli-Q water) was used in all experiments.

2.2. Preparation of R-CDs. Citric acid (1.2 g), *p*-phenylenediamine (0.5 g), and phytic acid (0.5 mL) are mixed in 80 mL of formamide under magnetic stirring for 30 min to form a transparent solution. Then, the solution was sealed in a poly(tetrafluoroethylene)-lined autoclave and heated at 180 °C for 4 h. After cooling down to room temperature, the obtained product was filtered through a filtration membrane (0.22 μm) to remove large particles. Subsequently, a proper amount of acetone was added to precipitate the CDs. Afterward, the obtained suspension was centrifuged to collect the precipitate (10,000 rpm, 10 min). The precipitate was washed with methanol/acetone mixtures several times and dried in vacuum.

2.3. Preparation of R-CDs/Starch Phosphors. R-CDs and starch were mixed by a mass ratio of 1:40 in methanol.[20,25] Then, the mixtures were sealed in a beaker with a plastic film under constant stirring for 24 h. The reaction mixtures were then collected by centrifugation (2000 rpm, 10 min) and dried in a vacuum oven to get the powder for further experiments.

2.4. Development and Imaging of LFPs. All fingerprints in this work were collected from a thumb of a man aged 25. He washed his hands with soap and water and then ran his fingers across his forehead and pressed his fingers on various substrates including glass, paper, and plastic pieces, respectively. As shown in Scheme 1, we developed these LFPs by the classical powder-dusting method. Specifically, R-CDs/starch powders were generally picked up using a feather brush and uniformly scattered onto the LFPs. Then, the redundant powders were gently removed using the brush. The bright red fluorescent patterns of fingerprints were seen clearly under a green light lamp. The pictures were taken using a digital camera equipped with an optical filter to filter green light (Figure S1).

To prepare a control, the same figure was rolled on the inking plate until the ink was covered from one edge of the nail to the other and from the crease of the first joint to the tip of the finger. Then, the finger was placed upon a fingerprint card and rolled from one side to the other until it faced the opposite direction. Finally, lift up the finger carefully to avoid smudging (Figure S2).[26] Afterward, the photographs were also taken using the same camera in the daylight.[3,27]

2.5. Benchmark. The classical cyanoacrylic acid-fuming method has been applied widely for 60 years. Typically, 0.1 g of rhodamine 6G was dissolved in a solution containing 100 mL of isopropyl alcohol, 150 mL of 2-butanone, and 750 mL of Milli-Q water. Then, the LFPs on a glass sheet were fumigated with cyanoacrylic acid using a fuming system (Figure S3A). Afterward, the glass sheet was immersed in the abovementioned rhodamine 6G solution for 15 s, followed by rinsing by deionized water. The glass sheet was dried at room temperature before taking photographs using a camera (Figure S3B).[3]

2.6. Characterizations. The transmission electron microscopy (TEM) images were taken using a JEM-2010 transmission electron microscope. The fluorescence spectra were recorded using a Horiba

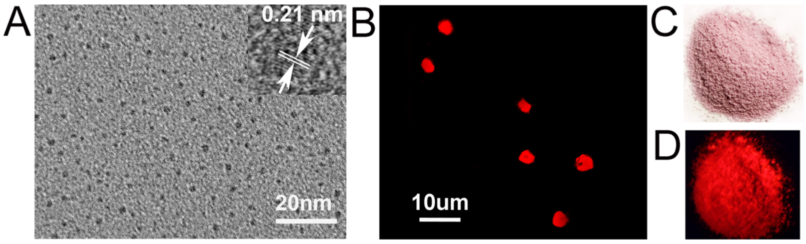

Figure 1. (A) TEM and HRTEM (inset) images of the R-CDs. (B) Confocal fluorescence image of the R-CDs/starch phosphors under green light excitation. Fluorescence images of the R-CDs/starch phosphors under (C) room light and (D) green light, respectively.

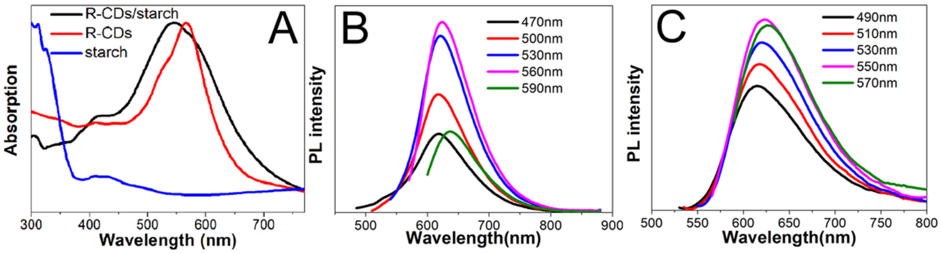

Figure 2. (A) UV−vis absorption spectra of starch, R-CDs, and R-CDs/starch phosphors. PL emission spectra of (B) R-CDs in methanol and (C) R-CDs/starch phosphors under excitation of different wavelengths, respectively.

Jobin Yvon fluormax-4 spectrofluorometer. The quantum yield was measured using an F-3018 quantum yield accessory including an integrating sphere. The UV−vis absorption spectra were measured on a Unico UV-2802 PC spectrometer. The diffuse reflectance spectra were measured using Lambda 650S with an integrating sphere scanning from 300 to 850 nm with $BaSO_4$ as the reference. Fourier transform infrared (FTIR) spectra were recorded on a Nicolet Nexus 470 FTIR spectrometer. X-ray photoelectron spectra (XPS) were recorded using an AXIS Ultra DLD spectrometer. Confocal fluorescence images were recorded using a Nikon C2+ laser scanning confocal microscope.

3. RESULTS AND DISCUSSION

Scheme 1 illustrates the roadmap of the whole study, which includes four steps: the preparation of R-CDs/starch powder, the development of LFPs, the image collection, and the computer processing. Although the first step takes about one day, the subsequent three steps only need several minutes, respectively. Hence, our work provides a rapid route for LFP identification at scenes. In comparison with many commercial fluorescent dyes, such R-CDs/starch powder exhibits good photoluminescent properties which overcome the background fluorescence of conventional substrates and specific adhesion toward LFPs that produces stable images for accurate identification. After careful development, the R-CDs/starch powder-stained LFPs could exhibit strong red fluorescence for months. To clarify the structures and properties, the as-prepared R-CDs and R-CDs/starch phosphors were characterized using various techniques and analyzed.

The TEM image (Figure 1A) shows that the R-CDs are monodispersed nanoparticles with an average diameter of about 2.3 nm, whereas the inset high-resolution TEM (HRTEM) image of R-CDs exhibits well-resolved lattice fringes with a spacing of 0.21 nm, corresponding to the (100) lattice space of graphene. After integration with starch, the obtained R-CDs/starch phosphors with particle sizes of about 5 μm exhibit uniform red fluorescence under green light excitation of a laser confocal microscope (Figure 1B), indicating that R-CDs have been adsorbed on starch homogeneously.[20,25] Such an R-CDs/starch powder is pale pink in the daylight (Figure 1C) and emits bright red fluorescence under the UV light (Figure 1D). The FTIR spectra of R-CDs (Figure S4A) show stretching vibrations of O−H at 3423 cm^{-1}, N−H at 3243 cm^{-1}, C=O at 1705 cm^{-1}, C=N at 1635 cm^{-1}, C=C at 1512 cm^{-1}, and C−N at 1390 cm^{-1}, which are also observed in the FTIR spectra of R-CDs/starch (Figure S4B). This phenomenon indicates that R-CDs are coated around starch particles. Thus, the abovementioned functional groups of R-CDs, which are the basis of adsorption effects between R-CDs and the fingerprint residues,[28−30] will work at full capacity.

The UV−visible absorption spectra of starch, R-CDs, and R-CDs/starch phosphors are compared, as shown in Figure 2A. In the visible region, the starch powder has almost no absorption while R-CDs show the main absorption peak at about 570 nm. When starch and R-CDs integrate together, this peak blue shifts to about 550 nm and becomes broader. This interesting phenomenon is worthy of discussion. On the one hand, nanoparticles aggregate together in a solid powder and the molecular orbitals of CDs will overlap with each other nearby. Such a molecular orbital overlap will decrease the average band gaps of CDs and induce a red shift of the absorption curve. However, when R-CDs are dispersed into 40 times of starch, the average distance between CDs is enlarged significantly, so the abovementioned red shift will be suppressed and the absorption curve exhibits a blue shift. On the other hand, the absorption of CDs in the visible region mainly arises from their surface states. When the molecular orbitals of R-CDs' surface groups couple with those of starch, the electrons of R-CDs will have more excited state levels, so they are able to absorb light with a wider wavelength range. Therefore, both the peak blue-shifting and the absorption spectrum broadening indicate strong interactions between R-CDs and starch.[20,25] In Figure 2B, R-CDs show the typical excitation-independent PL emission in methanol solution, with a peak at about 620 nm. This character is inherited by R-CDs/starch, although starch has no fluorescence itself (Figure 2C). As shown in normalized PL spectra of R-CDs in methanol and R-CDs/starch phosphors (Figure S5A,B), with the increase in

https://dx.doi.org/10.1021/acsami.0c01972
ACS Appl. Mater. Interfaces 2020, 12, 29549−29555

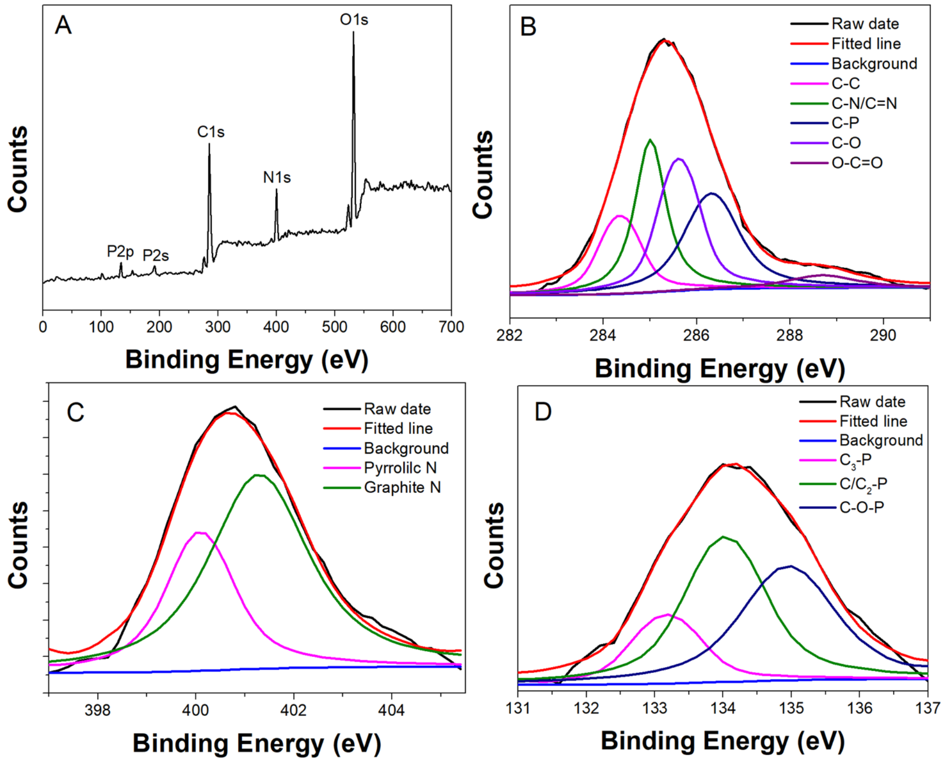

Figure 3. XPS spectra of (A) R-CDs and the deconvoluted details (B) C 1s, (C) N 1s, and (D) P 2p, respectively.

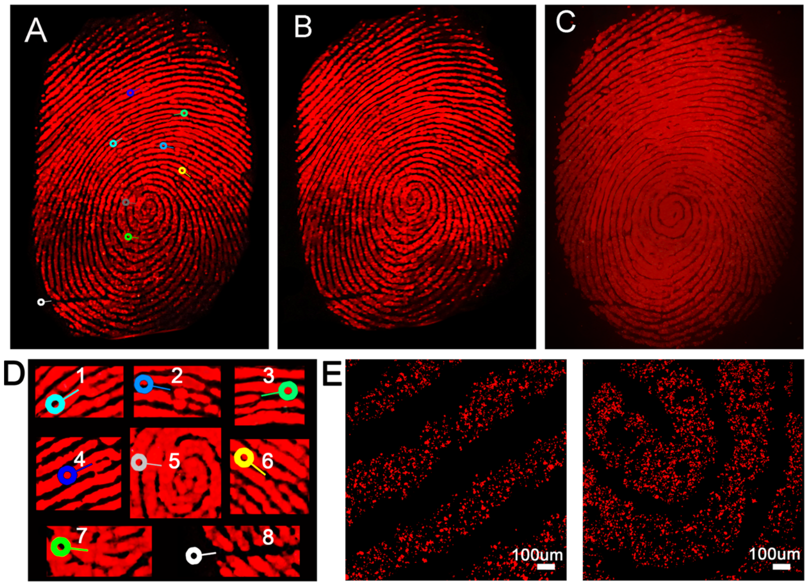

Figure 4. Photographs of the R-CDs/starch phosphor-stained LFPs on (A) glass, (B) paper, and (C) plastic substrates under green light irradiation, respectively. (D) Magnified images showing eight kinds of details as marked in A, that is, (1) bifurcation, (2) island, (3) termination, (4) eye, (5) core, (6) ridge divergence, (7) crossover, and (8) scar. Confocal fluorescence images of (E) R-CDs/starch-stained fingerprints on a glass sheet and (F) same sample after several weeks' storage.

excitation wavelength, the position of the emission peak hardly changed, which revealed that both R-CDs in solution and R-CDs/starch phosphors exhibit the excitation-independent PL emission. When the R-CD solution is dried into powder, its fluorescence becomes very weak because of the concentration quenching effects. In contrast, the PL quantum yield (PLQY) of the R-CDs/starch phosphors, measured using an integrating sphere under 550 nm of excitation, is around 21%, much higher than many other solid-state CDs (Table S1).[22,23,31,32]

The XPS of R-CDs in the full range (Figure 3A) show the bands of C 1s, N 1s, O 1s, P 2s, and P 2p and the element compositions of 73.48, 19.37, 5.87, and 1.28% for C, O, N, and P, respectively. In the high-resolution XPS, the C 1s band (Figure 3B) can be deconvoluted into five peaks of C−C at 284.4 eV, C−N/C═N at 285.0 eV, C−O at 285.6 eV, C−P at 286.4 eV, and O−C═O at 288.7 eV. The N 1s spectrum (Figure 3C) displays two peaks at 400.0 and 401.2 eV, attributed to the pyrrolic C_2−N−H and the graphitic N−C3,

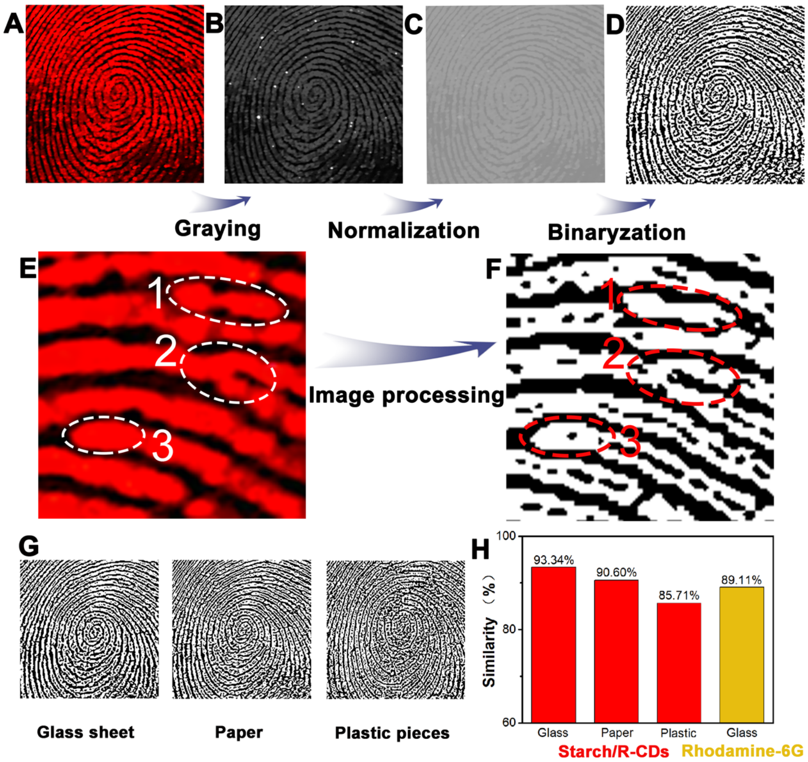

Figure 5. Image digital-processing procedure of LFPs on paper, from (A) input image, (B) grayscale image, and (C) normalized image to (D) binary image. The second-level details, (1) island, (2) bifurcation, and (3) termination in the partially enlarged images, are converted from (E) input image to (F) binary image, respectively. (G) Binary images of fingerprints on three different substrates. (H) Similarity assessment results of the same fingerprint on different substrates and the benchmark obtained by the standard fuming method.

respectively. The P 2p band (Figure 3D) contains three peaks at 133.2, 134.0, and 135.0 eV attributed to C_3−P, C/C_2−P, and C−O−P, respectively. It is known that defects induced by N and P codoping can lead to a highly localized state close to the Fermi level and affect the degree of graphitization of CDs.[33] As a result, our CDs emit strong red fluorescence which forms high contrast with the background fluorescence of most substrates so as to facilitate LFP detection.

To test the function of R-CDs/starch phosphors for LFP detection, three typical substrates, including glass, paper, and plastic pieces, were selected (Figure S6). Before LFP detection, we have optimized the mass ratios between R-CDs and starch according to the quantum yield of the R-CDs/starch phosphors (Table S2). It is found that the R-CDs/starch with a mass ratio of 1:40 has the highest PLQY. As shown in Figure 4A−C, LFPs are detected successfully on all substrates. The ridge patterns of all samples, such as arches, loops, and whorls, classified in level one, are recognized clearly because of the high contrast of fluorescent signals. It is well-known that the feature points in level two assign uniqueness and invariance to fingerprints through random combinations, which provide the most important identification information in fingerprint analyses. In Figures 4A,D, these feature points are observed clearly and marked as (1) bifurcation, (2) island, (3) termination, (4) eye, (5) core, (6) ridge divergence, and (7) crossover, respectively. In general, the feature points in level three provide vital reference information when particular defects occur and/or level two signals are blurred, although they cannot be used to identify LFPs alone.[34] In the present fingerprint image, a (8) scar is found and assigned to level three. Because the present LFP possesses all information of three levels, it is perfect for further analyses. The confocal fluorescence images of this LFP on a glass sheet (Figure 4E) clearly show the red-emissive R-CDs/starch particles, which adhere on the finger residues and illustrate the LFP details precisely. Even after several weeks' storage, such a fluorescence image is still bright and clear (Figure 4F).

As one of the artificial intelligence techniques, the digital processing by MatLab has become an important tool for analyzing LFP images.[35,36] This method is based on the minutiae features which are derived from the local information points inherent in fingerprint images using a computer program. The original LFP image should be distinguishable enough, which means that it has clear feature structures of both the level 1 and level 2. Before extracting feature points, the original image of a fingerprint is converted into a binary model by three steps.[4,5,37,38] At first, the input color image (Figure 5A) is converted to a grayscale image (Figure 5B). Then, the image is normalized to highlight the target outline (Figure 5C). Finally, binaryzation is conducted through dividing different pixels into two types “1” or “0” according to their grayscale values (Figure 5D), that is, each pixel of the image is redrawn as white (1) or black (0). After binaryzation, these noise points and shadows disappear while the vague areas are sharpened. In more details, from Figure 5E,F, the level two features of LFPs including islands, bifurcations, and ridge terminations have been successfully preserved and enhanced. In this way, LFP images on different substrates (glass, paper, and plastic) are converted (Figure 5G) and compared with the control. The control is obtained by directly pressing the same finger on a fingerprint card with black ink according to the standards of the Federal Bureau of Investigation.[26] In general, details of the control must be clear enough to define the loop, whorl, arch, or other features.

For our present samples, seven kinds of feature points are found by the Galton-Henry Classification after binaryzation (Figure S7), containing island (1), bifurcation (2, 5, 6, and 7), and termination (3) and (4).[3,17,39] Before comparison, the feature point coordinates are extracted from a binary image and transformed to "m × 2" values so as to make a matrix. As eq 1 shows, Z is the matrix of the sample while X is the matrix of the control.

$$Z = \begin{bmatrix} z_{11} & z_{12} \\ \vdots & \vdots \\ z_{i1} & z_{i2} \\ \vdots & \vdots \\ z_{m1} & z_{m2} \end{bmatrix}, \qquad X = \begin{bmatrix} x_{11} & x_{12} \\ \vdots & \vdots \\ x_{i1} & x_{i2} \\ \vdots & \vdots \\ x_{m1} & x_{m2} \end{bmatrix} \tag{1}$$

$$P = \frac{1}{m}\sum_{i=1}^{m} \frac{1}{\left| \frac{\sqrt{(z_{i1}-a)^2 + (z_{i2}-b)^2}}{\sqrt{(x_{i1}-a)^2 + (x_{i2}-b)^2}} - 1 \right| + 1}, \quad (i = 1, 2, 3 \ldots, m) \tag{2}$$

To quantify the similarity between the sample and the control, the Euclidean Distance Formula is used to calculate the similarity between fingerprint characteristic matrixes using eq 2.[5,6,37,40,41] In the collected values, (z_{i1}, z_{i2}) and (x_{i1}, x_{i2}) are the feature point coordinates and (a, b) is the coordinate of the image core point. When the matching score P equals to 1, these two matrixes are exactly the same. Obviously, the larger the matching score, the higher the similarity. Using eq 2 to calculate the matching scores of our samples, the computer program presents the results of 93.34, 90.60, and 85.71% for LFPs on glass, paper, and plastic substrates, respectively (Figure 5H). As a benchmark, the standard cyanoacrylic acid-fuming method applied by the police is also employed to stain our LFPs with rhodamine 6G on a glass sheet (Figure S3).[3] After evaluation using our digital program, the matching score of this benchmark is 89.11% (Figure S8). Therefore, the perfect combination of R-CD phosphors and the artificial intelligence program has shown significant progress over the traditional method for LFP identification.

4. CONCLUSIONS

We invent a new method of utilizing R-CDs/starch as a dusting powder for developing LFPs and establish an artificial intelligence program to evaluate the similarity of the developed LFP images quantitatively. In comparison with those previous reports concerning fluorescent detection of LFPs, our present work achieves significant progress in the following aspects. First, the low-cost R-CDs/starch phosphors overcome the conventional CD fluorescence quenching induced by aggregation and drying and exhibit a high PLQY of 21% in the solid state. Second, the luminescent color of our phosphors is red, which avoids the interference of background fluorescence in most cases, and thus, the signal accuracy of the stained LFPs can be improved effectively. Third, both the R-CDs/starch preparation and the LFP development are simple, safe, fast, portable, and widely compatible, much better than the traditional procedures such as the fuming method. Finally, a digital-processing program is designed for handling and comparing the LFP images. The feature points of LFPs are well-preserved and enhanced after image processing, and the similarity between the sample and the control can be evaluated quantitatively and objectively just by the matching score. An excellent matching score of 93% in our study shows great improvement over the traditional benchmark, which confirms that our material and method can be applied for LFP detection and identification practically.

■ ASSOCIATED CONTENT

Supporting Information

The Supporting Information is available free of charge at https://pubs.acs.org/doi/10.1021/acsami.0c01972.

Additional characterization results of FTIR, XPS, imaging systems, benchmarks, computer processing, and comparison results (PDF)

■ AUTHOR INFORMATION

Corresponding Author

Huan-Ming Xiong − *Department of Chemistry and Shanghai Key Laboratory of Molecular Catalysis and Innovative Materials, Fudan University, Shanghai 200438, P. R. China;* orcid.org/0000-0002-3118-942X; Email: hmxiong@fudan.edu.cn

Authors

Xiang-Yang Dong − *Department of Chemistry and Shanghai Key Laboratory of Molecular Catalysis and Innovative Materials, Fudan University, Shanghai 200438, P. R. China*

Xiao-Qing Niu − *Department of Chemistry and Shanghai Key Laboratory of Molecular Catalysis and Innovative Materials, Fudan University, Shanghai 200438, P. R. China*

Zheng-Yong Zhang − *School of Management Science and Engineering, Nanjing University of Finance and Economics, Nanjing, Jiangsu 210023, P. R. China*

Ji-Shi Wei − *Department of Chemistry and Shanghai Key Laboratory of Molecular Catalysis and Innovative Materials, Fudan University, Shanghai 200438, P. R. China*

Complete contact information is available at: https://pubs.acs.org/10.1021/acsami.0c01972

Notes

The authors declare no competing financial interest.

■ ACKNOWLEDGMENTS

This work was financially supported by the National Natural Science Foundation of China (Grant nos. 21771039, 21975048, and 61602217) and the Shanghai Science and Technology Committee (no. 19DZ2270100).

■ REFERENCES

(1) Odén, S.; Hofsten, B. V. Detection of fingerprints by the ninhydrin reaction. *Nature* **1954**, *173*, 449−450.

(2) Hazarika, P.; Russell, D. A. Advances in fingerprint analysis. *Angew. Chem., Int. Ed.* **2012**, *51*, 3524−3531.

(3) Champod, C.; Lennard, C. J.; Margot, P.; Stoilovic, M. *Fingerprints and Other Ridge Skin Impressions*; CRC Press: Boca Raton, Florida, USA, 2004.

(4) Maltoni, D.; Jain, A. K.; Maio, D.; Prabhakar, S. *Handbook of Fingerprint Recognition*; Springer Verlag: London, England, 2009.

(5) Bhanu, B.; Tan, X. *Computational Algorithms for Fingerprint Recognition*; Kluwer Academic: New York, USA, 2004.

(6) Qi, J.; Wang, Y. A robust fingerprint matching method. *Pattern Recogn.* **2005**, *38*, 1665−1671.

(7) Ramotowski, R. *Lee and Gaensslen's Advances in Fingerprint Technology*; CRC Press: Boca Raton, Florida, USA, 2013.

(8) Ifa, D. R.; Manicke, N. E.; Dill, A. L.; Cooks, R. G. Latent fingerprint chemical imaging by mass spectrometry. *Science* **2008**, *321*, 805.

(9) Xu, L.; Li, Y.; Wu, S.; Liu, X.; Su, B. Imaging latent fingerprints by electrochemiluminescence. *Angew. Chem., Int. Ed.* **2012**, *51*, 8068−8072.

(10) Wolfbeis, O. S. Nanoparticle-enhanced fluorescence imaging of latent fingerprints reveals drug abuse. *Angew. Chem., Int. Ed.* **2009**, *48*, 2268−2269.

(11) Xu, L.; Zhang, C.; He, Y.; Su, B. Advances in the development and component recognition of latent fingerprints. *Sci. China Chem.* **2015**, *58*, 1090−1096.

(12) Baker, S. N.; Baker, G. A. Luminescent carbon nanodots: emergent nanolights. *Angew. Chem., Int. Ed. Engl.* **2010**, *49*, 6726−6744.

(13) Ryu, S.-J.; Jung, H.-S.; Lee, J.-K. Latent Fingerprint Detection using Semiconductor Quantum Dots as a Fluorescent Inorganic Nanomaterial for Forensic Application. *Bull. Korean Chem. Soc.* **2015**, *36*, 2561−2564.

(14) Wang, J.; Wei, T.; Li, X.; Zhang, B.; Wang, J.; Huang, C.; Yuan, Q. Near-infrared-light-mediated imaging of latent fingerprints based on molecular recognition. *Angew. Chem., Int. Ed.* **2014**, *53*, 1616−1620.

(15) Chen, J.; Wei, J.-S.; Zhang, P.; Niu, X.-Q.; Zhao, W.; Zhu, Z.-Y.; Ding, H.; Xiong, H.-M. Red-Emissive Carbon Dots for Fingerprints Detection by Spray Method: Coffee Ring Effect and Unquenched Fluorescence in Drying Process. *ACS Appl. Mater. Interfaces* **2017**, *9*, 18429−18433.

(16) Lou, Q.; Qu, S.; Jing, P.; Ji, W.; Li, D.; Cao, J.; Zhang, H.; Liu, L.; Zhao, J.; Shen, D. Water-triggered luminescent "nano-bombs" based on supra-(carbon nanodots). *Adv. Mater.* **2015**, *27*, 1389−1394.

(17) Jain, A. K.; Flynn, P.; Ross, A. A. *Handbook of Biometrics*; Springer US: New York, USA, 2007.

(18) Lu, S.; Sui, L.; Liu, J.; Zhu, S.; Chen, A.; Jin, M.; Yang, B. Near-Infrared Photoluminescent Polymer-Carbon Nanodots with Two-Photon Fluorescence. *Adv. Mater.* **2017**, *29*, 1603443.

(19) Zhu, C.; Fu, Y.; Liu, C.; Liu, Y.; Hu, L.; Liu, J.; Bello, I.; Li, H.; Liu, N.; Guo, S.; Huang, H.; Lifshitz, Y.; Lee, S. T.; Kang, Z. Carbon Dots as Fillers Inducing Healing/Self-Healing and Anticorrosion Properties in Polymers. *Adv. Mater.* **2017**, *29*, 1701399.

(20) Qu, S.; Zhou, D.; Li, D.; Ji, W.; Jing, P.; Han, D.; Liu, L.; Zeng, H.; Shen, D. Toward Efficient Orange Emissive Carbon Nanodots through Conjugated sp(2) -Domain Controlling and Surface Charges Engineering. *Adv. Mater.* **2016**, *28*, 3516−3521.

(21) Pan, L.; Sun, S.; Zhang, A.; Jiang, K.; Zhang, L.; Dong, C.; Huang, Q.; Wu, A.; Lin, H. Truly Fluorescent Excitation-Dependent Carbon Dots and Their Applications in Multicolor Cellular Imaging and Multidimensional Sensing. *Adv. Mater.* **2015**, *27*, 7782−7787.

(22) Xu, M.; He, G.; Li, Z.; He, F.; Gao, F.; Su, Y.; Zhang, L.; Yang, Z.; Zhang, Y. A green heterogeneous synthesis of N-doped carbon dots and their photoluminescence applications in solid and aqueous states. *Nanoscale* **2014**, *6*, 10307−10315.

(23) Fernandes, D.; Krysmann, M. J.; Kelarakis, A. Carbon dot based nanopowders and their application for fingerprint recovery. *Chem. Commun.* **2015**, *51*, 4902−4905.

(24) Zhao, D.; Ma, W.; Xiao, X. The Recognition of Sweat Latent Fingerprints with Green-Emitting Carbon Dots. *Nanomaterials* **2018**, *8*, 612.

(25) Sun, M.; Qu, S.; Hao, Z.; Ji, W.; Jing, P.; Zhang, H.; Zhang, L.; Zhao, J.; Shen, D. Towards efficient solid-state photoluminescence based on carbon-nanodots and starch composites. *Nanoscale* **2014**, *6*, 13076−13081.

(26) Hoover, J. E. *The Science of Fingerprints*; Federal Bureau of Investigation: USA, 1945; pp 1−190.

(27) Henderson, C.; Lenz, K. W. Legal Issues Concerning Expert Evidence and Testimony. *The Forensic Laboratory Handbook Procedures and Practice*; Springer, 2011.

(28) Song, K.; Huang, P.; Yi, C.; Ning, B.; Hu, S.; Nie, L.; Chen, X.; Nie, Z. Photoacoustic and Colorimetric Visualization of Latent Fingerprints. *ACS Nano* **2015**, *9*, 12344−12348.

(29) Choi, M. J.; McDonagh, A. M.; Maynard, P.; Roux, C. Metal-containing nanoparticles and nano-structured particles in fingermark detection. *Forensic Sci. Int.* **2008**, *179*, 87−97.

(30) Li, Y.; Xu, L.; Su, B. Aggregation induced emission for the recognition of latent fingerprints. *Chem. Commun.* **2012**, *48*, 4109−4111.

(31) Wang, H.; Sun, X.; Zhang, T.; Chen, X.; Zhu, J.; Xu, W.; Bai, X.; Dong, B.; Cui, H.; Song, H. Photoluminescence enhancement of carbon dots induced by hybrids of photonic crystals and gold−silver alloy nanoparticles. *J. Mater. Chem. C* **2018**, *6*, 147−152.

(32) He, J.; He, Y.; Chen, Y.; Lei, B.; Zhuang, J.; Xiao, Y.; Liang, Y.; Zheng, M.; Zhang, H.; Liu, Y. Solid-State Carbon Dots with Red Fluorescence and Efficient Construction of Dual-Fluorescence Morphologies. *Small* **2017**, *13*, 1700075.

(33) Sun, X.; Brückner, C.; Lei, Y. One-pot and ultrafast synthesis of nitrogen and phosphorus co-doped carbon dots possessing bright dual wavelength fluorescence emission. *Nanoscale* **2015**, *7*, 17278−17282.

(34) Singh, P.; Singh, H.; Sharma, R.; Bhargava, G.; Kumar, S. Diphenylpyrimidinone−salicylideneamine − new ESIPT based AIEgens with applications in latent fingerprinting. *J. Mater. Chem. C* **2016**, *4*, 11180−11189.

(35) Sudiro, S.; Puspa, I.; Wardijono, B.; Handias, B. Fingerprint matching application using hardware based artificial neural network with Matlab. In *5th International Conference on Electrical, Electronics and Information Engineering (ICEEIE)*, Malang, 2017; pp 66−70.

(36) Swarup, A.; Dheeraj, K.; Kumar, A. In *Fingerprint-Based Attendance System Using MATLAB*, Singapore; Springer Singapore: Singapore, 2017; pp 999−1004.

(37) Adhiyaman, M.; Ezhilmaran, D. Fingerprint Matching and Similarity Checking System using Minutiae Based Technique. In *2015 IEEE International Conference on Engineering and Technology (ICETECH)*, Coimbatore, 2015.

(38) Zhang, D.; Jain, A. K. *Advances in Biometrics*; Springer Verlag: Heidelberg, Berlin, Germany, 2006; pp 213−348.

(39) Jain, A. K.; Yi, C.; Meltem, D. Pores and ridges: high-resolution fingerprint matching using level 3 features. *IEEE Trans. Pattern Anal. Mach. Intell.* **2007**, *29*, 15.

(40) Pornpanomchai, C.; Phaisitkulwiwat, A. Fingerprint Recognition by Euclidean Distance. In *Second International Conference on Computer and Network Technology*, Bangkok, 2010; pp 437−441.

(41) Bhowmik, U. K.; Ashrafi, A.; Adhami, R. R. A Fingerprint Verification Algorithm Using the Smallest Minimum Sum of Closest Euclidean Distance. In *2009 International Conference on Electrical, Communications, and Computers*, Cholula, 2009; pp 90−95.